CO2 Capture by TiO2 Anatase Surfaces: A Combined DFT and FTIR Study

CO_2 Capture by TiO_2 Anatase Surfaces: a Combined DFT and FTIR Study

L. Mino, G. Spoto, A.M. Ferrari

J. Phys. Chem. C (2014), 118, 25016 − 25026

DOI: 10.1021/jp507443k

CO_2 Capture by TiO_2 Anatase Surfaces: a Combined DFT and FTIR Study

Lorenzo Mino, Giuseppe Spoto, Anna Maria Ferrari[1]
Department of Chemistry, NIS Centre of Excellence, University of Turin, via P. Giuria 7, 10125 Torino, Italy

Abstract

In this work, by combining FTIR results with periodic DFT calculations, we highlight the role of different anatase surface sites in the CO_2 adsorption and in the subsequent reactions. It is shown that CO_2 is mainly adsorbed in linear form at the (101) surface, while the formation of a variety of surface carbonates is occurring at the (001) one. The role of co-adsorbed water in the formation of surface bicarbonates is also investigated. All the structures identified by FTIR spectroscopy were modeled by DFT and the adsorption geometries and the energy of formation for the surface species were carefully analyzed. For the most stable structures we also performed the calculation of the vibrational frequencies that were compared with the FTIR data.

Keywords: vibrational spectroscopy, *ab initio* modeling, hydroxyl groups, surface carbonates, TiO_2 anatase nanoparticles

[1] Anna Maria Ferrari
Dipartimento di Chimica
Università di Torino
Via P. Giuria 5 10125 Torino Italy
Email: anna.ferrari@unito.it

1) Introduction

The increase of concentration of carbon dioxide in the atmosphere is one of the major contributors (together with methane and CFC) to the greenhouse effect and the consequent global warming. The main reason of the atmospheric CO_2 increase is ascribed to anthropic activities related to combustion of fossil fuels.[1] Several strategies have been indicated in order to deal with CO_2 management: i) reduction of CO_2 emission that is driving innovative research projects towards CO_2 neutral energetic technologies, (hydrogen as fuel or energy vector, photovoltaics, wind farms, etc…); ii) CO_2 sequestration and storage strategies similar to those adopted for radioactive waste;[2] iii) chemical fixation on reactive substrate like metals and metal oxides.[3] This latter approach appears to have a great potential and has gained an increasing attention in the last decade, since it combines the possibility to produce, through (photo)catalytically driven reactions, raw materials and valuable chemicals, together with a substantial mitigation of the greenhouse effect.[4]

Among various catalysts proposed, TiO_2-based materials have been considered the most appropriate candidate for photocatalytic processes due to their powerful oxidation properties, superior charge transport properties, and corrosion resistance. In 1979 Honda and coworkers reported the photoreduction of CO_2 to form formic acid, formaldehyde, methyl alcohol and methane in aqueous suspension of semiconductors such as TiO_2, once the suspension had been illuminated with light absorbable by the catalyst.[5] After this pivotal work, many attempts to improve the efficiency of the photoreaction have been made over the past few decades. In this respect, several strategies have been adopted including the use of metal particles as co-catalyst,[6,7] the modulation of the electron structure of the oxide by dopants,[8] the use of organic molecules as sensitizers[7] and the nanostructuration of the materials.[9,10]

Despite such a considerable amount of studies, the conversion efficiency of CO_2 into useful hydrocarbons is still too low for technological applications. Further progress requires the understanding of the (photo)reduction processes at the atomic level that cannot be obtained without a detailed knowledge of how CO_2 interacts with TiO_2. This implies a comprehension at the atomic level of the structure of the exposed surfaces, of their reactivity and of which is the bonding mechanism. To this extent, quantum chemical calculations have shown the unrivalled capability to elucidate at the atomistic level the mechanism of many phenomena involving surface reactivity. Nonetheless, in the case of CO_2/titania interaction, only a handful of simulations have been performed and almost only limited to the most stable (110) rutile and (101) anatase surfaces (see Refs. [11,12] and references therein). This finding is somewhat surprising since, for instance, in the case of anatase, Fourier transform infrared spectroscopy (FTIR) of adsorbed CO has highlighted a significant presence of the less stable (001) surface[13,14]. Furthermore, density functional theory

(DFT) calculations dealing with the interactions of anatase surfaces with small molecules such as water, ammonia and formic acid, have suggested a higher reactivity of the (001) surface over the most stable (101).[15,16] Finally, a recent combined FTIR and DFT study showed that the surface Ti sites exposed by the anatase (101) and (001) surfaces exhibit significantly different Lewis acidity and polarizing power, possibly resulting in different reactivity toward CO_2.[17]

In this paper we present a combined FTIR and periodic DFT study of the interaction of CO_2 with the (101) and (001) anatase surfaces. Carbon dioxide can interact with the surface acid Lewis centers through the O ends but can also interact with the surface basic Lewis center through the C atom leading to the formation of surface carbonates; on hydrated surfaces the interaction with the exposed hydroxyls may produce bicarbonates. In this respect CO_2 can be also considered as a valuable probe to evaluate the basicity of the surface oxygen centers.

The surface structures possibly deriving from CO_2 adsorption on TiO_2 usually considered in the literature are sketched in **Scheme 1**.[18-21] They can grouped in: i) linear structures (**L**) that include, considering the orientation of the molecule with respect to the surface, parallel and perpendicular configurations; ii) monodentated carbonates (**MC**) that can be conceived of two types: a carbonate coordinated to a surface Ti center or a sort of "surface" carbonate in which one the oxygen of the $-CO_3$ moiety is itself a surface oxygen kept nearly fixed at its lattice position; iii) bidentated carbonates (**BC**) that can be divided into bridging BC, where the carbonate is bound to two adjacent Ti centers, and chelating BC, where the bidentated bond is with a single Ti center; iv) modentated and bidentated bicarbonates (**MB** and **BB**) derived from the corresponding carbonate structures.

We modeled all the relevant structures and we carefully analyzed the relative adsorption geometries and energetics involved in the formation of the surface species. For the most stable structures we performed the calculation of the vibrational spectra which were compared with the experimental ones recorded at room temperature. Combining experimental and theoretical results, we were able to rationalize the different reactivity of the two surfaces under analysis.

2) Experimental and computational details

Computational parameters. The CO_2 adsorption at the (001) and (101) anatase surfaces has been modeled employing the periodic CRYSTAL09 code,[22] using the hybrid PBE0 DFT functional.[23] Indeed, the PBE0 functional has been reported to give accurate structural and electronic properties for TiO_2 crystals;[24] in addition a recent report concerning the interaction of CO with TiO_2 nanocrystals has demonstrated that the selected functional is able to provide a feasible description of the energetic and the vibrational properties of the surface adsorbates.[17]

In the CRYSTAL code, the level of accuracy in evaluating the Coulomb and the exchange series is controlled by five parameters[22] for which 10^{-7}, 10^{-7}, 10^{-7}, 10^{-7}, 10^{-18} values have been used for all calculations. The convergence threshold for SCF energy was set to 10^{-9} Ha. The reciprocal space was sampled according to a regular sublattice determined by the shrinking factor[22] which was ranged from 2 to 6 (4 to 20 independent k-points in the irreducible part of the Brillouin zone) depending on the dimension of the adopted cell.

The surfaces of crystals were modeled with bidimensional slabs characterized by two infinite dimensions (x, y) and a finite thickness. Different CO_2 coverages were considered and modeled by employing supercell of appropriate size; we define the coverage θ as the ratio between the number of adsorbed molecules and the number of surface fivefold coordinated Ti sites. For θ=0.25 and 0.5, 2*x*2 and $\sqrt{2}x\sqrt{2}$ supercells have been built up, respectively, whereas θ=1 corresponds to the 1*x*1 cell. The thickness of the slab was set to about 8-10 Å (6 Ti-layers) since our previous report has proven that slabs of this thickness provide negligible differences in the adsorbed CO properties (i.e. binding energy, variation in the CO bond length, CO stretching frequencies) with respect to thicker slabs.[17]

Concerning the basis set, to find an appropriate compromise between accuracy and computational cost, the CO_2 molecule was described with a TZ-P basis set, the surface O and Ti atoms with a [511111-411-1] basis set resulting in (6s/3p/1d) and a [84211-631-411]/(5s/3p/3d) respectively; while a [8-411-1]/(1s/3sp/1d) and a HW/411-31/(3sp/2d), exploiting the Hay-Wadt small-core pseudopotential,[25] have been employed for the inner O and Ti atoms respectively. This basis set combination was already employed in our previous CO/anatase investigation and the associated basis set superposition error (BSSE) did not exceed 1.5 kcal mol^{-1}.[17]

The geometry optimization has been performed relaxing all the atoms in the cell and keeping fixed the lattice parameters at the bulk values. All the symmetry constraints have been removed. Adsorbate frequencies have been computed at the Γ point, within the harmonic approximation, by diagonalizing the mass-weighted Hessian matrix only for the adsorbate fragment, once checked that its vibrational modes are not coupled with other crystal phonons. Computed frequencies have been scaled by a factor 0.9525 in order to facilitate comparison with experiments. The scaling factor has been determined by matching for gas phase CO_2 the calculated $\nu_{AS}(CO)$ = 2466 cm^{-1} to the experimental value, $\nu_{AS}(CO)$ = 2349 cm^{-1}.

FTIR spectroscopy. TiO_2 anatase nanopowder (hereafter nanoanatase) was purchased from Sigma-Aldrich. The rutile content of the material, evaluated considering the relative intensity of the rutile

(110) and of the anatase (101) diffraction peaks,[26] was below 3%. The BET surface area was found to be 140 m^2/g.

Before CO and CO_2 adsorption the TiO_2 samples, in form of thin self-supporting pellet suitable for transmission FTIR measurements, were outgassed under high vacuum (residual pressure < 10^{-4} mbar) at 823 K in the same cryogenic cell (a properly modified closed circuit liquid helium Oxford CCC 1204 cryostat) allowing the infrared investigation of species adsorbed in controlled temperature (between 300 and 14 K) and pressure conditions. The thermal treatment was followed by an oxidation step at 723 K with 15 mbar of O_2 in order to obtain fully stoichiometric TiO_2.

The infrared spectra were recorded on a Bruker Equinox 55 FTIR spectrometer, equipped with an MCT cryogenic detector, with the sample compartment modified to accommodate the cryogenic head; 128 interferograms (recorded at 2 cm^{-1} resolution) were typically averaged for each spectrum.

3) Results from periodic DFT calculations.

a) Modeling the CO_2 interaction with the dry surfaces

The (001) surface. The surface is characterized by the presence of Ti(5f) and O(2f) atoms, see **Figure S1** of Supplementary Information. At this surface, the formation of linearly adsorbed CO_2 (**L**) together with the formation of mono (**MC**) and bidentated (**BC**) carbonates has been hypothesized (see **Scheme 1**). Considering the linear configurations, we found that the favored adsorption structures depend on the coverage. At low coverage (θ=0.25), the molecule adopts a flat configuration (001-L1) and is located between two facing Ti-O-Ti bridged moieties (**Figure 1)**. Increasing the coverage, the parallel arrangement, because of its steric hindrance, cannot be any longer accommodated on the surface, and the molecule moves to a linear perpendicular configuration. At θ=1, the stable configuration, 001-L2, is characterized by a O atom of the molecule bound to a surface Ti(5f) site (d(TiO)=2.92 Å); the bond is considerably tilted with respect to the normal to the surface, α(Ti-O-C)=130° and $d(O_SC)$=3.42 Å, see **Table 1**. In both configurations, CO_2 retains almost entirely its gas phase geometry, d(CO)~1.157 Å, the same bond distance as in the free molecule, and α(O-C-O) ~179°. The interaction with the surface is rather weak, ΔE_{form}=-5.3 and -3.4 kcal mol^{-1} for 001-L1 and 001-L2, respectively; the asymmetric CO stretching, 2336 (001-L1) and 2354 (001-L2) cm^{-1} is shifted by few wavenumbers with respect to the gas phase value, **Table 2**.

In the bent configuration, the CO_2 is bound to the surface through the C atom with a surface O site ($d(O_SC)$=1.31 Å) and through the O atoms that are bound to the surface Ti centers (d(TiO)=2.05 Å). It results in monodentate carbonate species (001-MC) indentified in **Scheme 1** as

"lattice MC" since one O from the TiO_2 lattice contributes to the formation of the carbonate moiety according to the reaction:

$$TiO_2 + CO_2 \rightarrow TiO\text{-}CO_3 \qquad (1)$$

The formation energy of surface carbonate is highly exothermic, ΔE_{form}= -30.1 kcal mol^{-1}, despite the energy cost to bent the molecule from its gas phase linear shape, 38.6 kcal mol^{-1}, and the considerably deformation that the surface undergoes. Indeed the O(2f) site moves inwards by about 0.6 Å and the Ti-O-Ti angle varies from 148° to 180° moving from the bare to the carbonated surface. The two adjacent Ti-O distances that in the free system are remarkably different, d(TiO) = 1.71 and 2.25 Å, become almost of the same length, d(TiO) = 2.09 Å, value considerable longer than in the inner layers, d(TiO) = 1.93 Å, where the lattice geometry resembles the bulk one.

The formation of very stable "lattice" carbonates at the (001) anatase surface was also reported in previous works.[27,28]

The CO_2 adsorption energy varies dramatically with the coverage: for θ=0.125 and 0.0625, ΔE_{form}= -46.7 and -48.1 kcal mol^{-1}. This strong dependence of ΔE_{form} on θ has been already highlighted in the case of MgO where at step sites CO_2 adsorption leads to surface carbonates whose ΔE_{form} varies from -28.8 to -52.11 kcal mol^{-1} by reducing θ from 0.67 to 0.33.[29] Nevertheless, the rationalization of this strong dependence of the adsorption energy on the CO_2 coverage requires an accurate analysis of the electron properties of the CO_2/TiO_2 interface that will be addressed in the last section.

Starting from the 001-MC structure, through a on-site rotation of the CO_3 moiety, a bridging bidentated carbonate (001-BC) can be conceived, **Scheme 1** and **Figure 1.** According to such arrangement the carbonate specie, that has originated by incorporating a bridging surface oxygen, is bound to two adjacent Ti surface sites through two oxygen atoms, leaving on the surface an oxygen vacancy. Although the final bonding with the surface is rather strong, ΔE_{form}= -20.9 kcal mol^{-1}, 001-BC is considerably less stable, by about 10 kcal mol^{-1}, than 001-MC. In addition this structure could not be localized for θ=0.5: in this case 001-BC spontaneously moves to 001-MC. We think therefore that 001-BC may be a metastable structure that, passing a very low barrier, can move to 001-MC.

Finally a bent structure, B1, with C pointing away from the surface has been considered, see **Scheme 1**. Our attempts to stabilize a 001-B1 structure were unsuccessful since B1 spontaneously moves to a linear shape. This finding is in agreement with recent results[30,31] concerning the anatase (101) surface, showing that the B1 structure could be localized at the reduced surface (even if unstable) but never at the neutral one.

The vibrational frequencies of the surface carbonates are reported in **Table 4** and compared with the corresponding values computed for a carbonate ion in $CaCO_3$, considered as representative of a free carbonate. The -CO_3 in $CaCO_3$ is characterized by a three-fold symmetry; the asymmetric stretching, IR active, is double degenerated and is located at ν_{AS}(CO)=1407 cm^{-1}, whereas the symmetric stretching, located at ν_{SS}(CO)=1086 cm^{-1}, is IR inactive.[32] With respect to the reference free carbonate, adsorption leads to the splitting of the double degenerate asymmetric stretching vibration that depends on the bonding properties at the interface, and to a tiny IR activity of the symmetric stretching. Indeed 001-MC and 001-BC are characterized by different and specific features; in 001-MC the ν_{as}(CO) splitting generates two components located at 1576 and 1376 cm^{-1} whereas for 001-BC the two components are located at 1802 and 1125 cm^{-1}.

*The (101) surface***.** The surface is characterized by the presence of both five-fold Ti(5f) and six-fold Ti(6f) coordinated Ti atoms and two-fold O(2f) and three-fold O(3f) coordinated O atoms, see **Figure S1** of Supplementary Information. At low coverage (θ=0.25), we have explored three different linear (101-L1, 101-L2, 101-L3) and two bent (101-B and 101-MC) configurations of adsorbed CO_2, see **Scheme 1** and **Figure 2**. 101-MC is the analogous for the 101 surface of the "lattice" carbonate already discussed in the case of the 001 one. In L1 and L2 the CO_2 molecule binds through one O atom to a surface Ti(5f) site (d(TiO)=2.62 and 2.54 Å, respectively) and with a bond contact with the closest surface O(2f) sites (d(O_SC)=3.10 and 2.99 Å, respectively); in configuration 101-L3 CO_2 lies in a plane that is roughly perpendicular with respect to the one containing L1 and L2 structures with the shortest bond contact with the surface d(TiO)=2.40 and d(O_SC)=3.3 Å. Indeed, in all the three configurations, the molecule is largely tilted relative to the surface normal, being the angle α(Ti-O-C)=149, 126 and 134° for 101-L1, 101-L2 and 101-L3, respectively. The adsorbed molecules are slightly deformed with respect to the gas phase structure since they retain almost entirely the linear structure, i.e. α(O-C-O) is close to 180° in all the three configurations, see **Table 3**. The 101-L1 configuration has the highest binding energy (ΔE_{form}= -9.5 kcal mol^{-1}), followed by 101-L2 and 101-L3 (ΔE_{form}= -7.8 and -8.5 kcal mol^{-1}, respectively). In the 101-B adsorption structure the molecule, bonded to adjacent Ti(5f) and O(2f) atoms, is largely deformed with respect to the linear shape, α(O-C-O) =131° and the surface configuration is not stable, ΔE_{form}=2.7 kcal mol^{-1}. The 101-MC configuration is even less stable than 101-B, by about 5 kcal mol^{-1} in agreement with previous periodic DFT calculations.[11,30] The order of stability of the surface structures, 101-L1>101-L2>101-B>101-MC is indeed similar to what obtained in the previous studies.[11,30] In particular, computed ΔE_{form}(101-L1) is quite close to the value of 11.05 kcal mol^{-1} determined using the more accurate PBE plus the Tkatchenko and Scheffler long range

dispersion corrections (PBE-TS) and also the higher stability of the most stable linear configuration, 101-L1, over the most stable bent one, 101-B, of about 10 kcal mol^{-1} well compares with the PBE-TS value (7 kcal mol^{-1}).[11]

The nearly unperturbed structure of adsorbed CO_2 in L1-L3 configurations is resembled in the CO_2 vibrational frequencies that remain close to the gas-phase values. The asymmetric CO stretching, 2359 (L1) and 2360 (L2) cm^{-1}, is blue-shifted with respect to the gas phase value; similar behavior can be recognized for the symmetric CO stretching, 1340 (L1) and 1336 (L2) cm^{-1} that becomes weakly IR active because of the polarizing effect of the surface (see **Table 2)**. The main effect of the increased coverage (θ=1) on the IR spectra, analyzed in the case of 101-L1, is a displacement of the vibrational frequencies by few wavenumbers (**Table 2)**.

b) Modeling the CO_2 interaction with partially hydrated surfaces

Water interacts with anatase in different ways depending on the surface involved in the adsorption and on the water coverage θ. On the (101) surface, from low coverage up to θ=1, water adopts a molecular form of adsorption; while on the (001) surface, from low coverage up to θ=0.5, water prefers a dissociated form of adsorption. At θ=1 water moves to a mixed state where half of the molecules are dissociated while the other half are molecularly adsorbed: the molecules that are not dissociated form a kind of "second layer" above the "first layer" of dissociated molecules.[15,33]

These observations are interesting since CO_2, once activated by the surface, can interact with hydroxyls to form surface bicarbonates according to the reaction:[11,12,34]

$$TiO_2\text{-}(OH_2) + CO_2 \rightarrow TiO_2\text{-}(OH)\text{-}HCO_3 \qquad (2)$$

This implies that in the experimental condition of a partially hydrated surface the (001) surface can lead to the formation of bicarbonate species. The resulting surface configurations can be grouped in modentated bicarbonates (MB) where the $–HCO_3$ interacts through one oxygen with one surface sites, and in bidentated bicarbonates (BB) where the $–HCO_3$ interacts through two oxygens with one or two adjacent Ti sites leading to either chelating or bridging structures, see **Scheme 1**.

*The (001) surface***.** The first step was the setup of a feasible model for the hydrated (001) anatase surface. The model adopted in this work, 001-OH, has been reported schematically in **Figure S2** of Supporting Information. In 001-OH, a quarter of water monolayer (θ=0.25) is adsorbed in a dissociative way on a Ti-O surface couple, resulting in the formation of hydrogen bonded hydroxyls. According to this model, the computed hydration energy E_{hyd}=-31.8 kcal mol^{-1} is in agreement with estimates from a previous work (E_{hyd}=-36.7 kcal mol^{-1}).[15]

In the case of a quarter of a monolayer of CO_2, θ=0.25, that impinges on a (001) surface hydrated by a quarter of monolayer of water (001-OH), different configurations of surface MB and BB were considered: they are reported in **Figure 3** and the most relevant adsorption properties are summarized in **Table 5**. Four different species of bidentated bicarbonates were analyzed, namely: 001-BB(1-3) of bridging type and 001-BB4 of chelating shape. These four configurations are the result of two slightly different reaction paths as reported in **Scheme 2**. According to reaction 2a, one CO_2 molecule interacts with a hydroxyl group leading to a bidentated bicarbonate and leaving on the surface a linear Ti-OH hydroxyls (001-BB1); according to reaction 2b, one CO_2 molecule interacts with a hydroxyl group leading to a bidentated bicarbonate either chelating or bridging and leaving on the surface a bridging hydroxyl (configurations 001-BB2-4). The bridging configurations are always more stable than the chelating one and indeed the order of stability is: ΔE_{form}(001-BB2) > ΔE_{form}(001-BB1)> ΔE_{form}(001-BB3) >ΔE_{form}(001-BB4). In the most stable configuration, 001-BB2, ΔE_{form}= -14.6 kcal mol^{-1}, the bicarbonate moiety is bound to two Ti sites adjacent to a O(3f) site; 001-BB3 differs from 001-BB2 only for the fact that the bicarbonate is bound to two Ti sites adjacent to a O(2f) site. In order to maximize the -HCO_3/oxide interaction at the interface, the O(2f) largely downshifts (by 0.8 Å) with respect to the bare surface, leading to a reduced stability of 001-BB3 over 001-BB2 by more than 10 kcal mol^{-1}, ΔE_{form}(001-BB3) = -4.3 kcal mol^{-1}, **Table 5**.

The vibrational frequencies of the surface bicarbonates are reported in **Table 4.** The most interesting features are the two ν_{AS}(CO) at 1620 and 1490-1440 cm^{-1}, which are quite shifted with respect to the MC species, and the –COH bending vibration, ν_B(COH), at about 1200 cm^{-1}.

Monodentated bicarbonates (see **Scheme 1**) are not stable on the surface since they spontaneously move to a bidentated configuration. However they can be stabilized by the interaction with surface hydroxyls. Three configurations of MB, namely 001-MB1-(3), have been hypothesized, which are reported in **Figure 3**. They differ for the local arrangement of hydrogen bonds between surface hydroxyls and bicarbonate. MB configurations are always less stable than BB and are all characterized by a non favorable formation energy, **Table 5.** The most stable structure 001-MB1 is characterized by ΔE_{form}= 0.1 kcal mol^{-1} followed by 001-MB2 with ΔE_{form}= 3.5 kcal mol^{-1}. The formation of MB specie cannot be ruled out on the basis of the slightly unfavorable formation energies since other effects have to be considered. First of all ΔE_{form} is largely affected by the model adopted to simulate the hydrated TiO_2 surface and in particular by the degree of hydration included in the model and by the localization of the hydroxyls groups on the surface. Secondly, on a partially hydrated surface hydroxyls are more likely localized at defective sites (steps, edges), a situation which is not completely accounted for by the model proposed in this work. On this kind of low-coordinated sites the ΔE_{form} of MB is reasonably expected to be larger.

The vibrational frequencies of 001-MB1 are reported in **Table 4.** The most interesting feature is the presence of a ν_{AS}(CO) at 1652 cm^{-1}, considerably shifted with respect to the BB structures, that can therefore provide a fingerprint for the identification of MB species.

*The (101) surface***.** As already pointed out, in the case of a partially hydrated surface, CO_2 retains its molecular shape and is not activated by the surface. The interaction with surface hydroxyls from adsorbed water is not expected to lead to a significant formation of bicarbonates. Therefore, the formation of surface bicarbonates on this surface was not considered.

4) FTIR spectroscopy of dehydroxylated surfaces

a) Study of the exposed surface sites by CO adsorption

To obtain an accurate picture of the surface of the nanoanatase sample in terms of exposed Lewis and Brønsted sites, we performed low temperature CO adsorption before studying the interaction of CO_2. Indeed, carbon monoxide provides information on the polarizing power of the exposed metal centers, on their two-dimensional arrangement and, indirectly, on the particle morphology since it is able to discriminate the Ti^{4+} sites present on different crystal faces.

The FTIR spectra, recorded at 60 K, of different CO coverages on dehydroxylated nanoanatase are reported in **Figure 4**. On the basis of the comprehensive set of periodic DFT calculations and experimental data thoroughly discussed in previous papers,[13,17,35] a complete assignment can be provided. Besides the band due to liquid-like CO centered at 2140 cm^{-1}, the spectra are dominated by the band centered at 2179 cm^{-1} which can be assigned to CO adsorbed on the (101) face. The nanocrystals expose also the less stable (001) surface, as testified by the presence of the weaker peak at 2166 cm^{-1}. Finally, the signal at 2208 cm^{-1} is due to CO adsorbed on highly acidic Ti Lewis sites exhibiting very low coordination like those located on edges, steps and corners. The presence of this band confirms that the sample is heavily dehydroxylated. However, few residual OH groups located on defect sites are still present and originate the broad band in the 2156-2158 cm^{-1} range.

b) CO_2 adsorption and comparison with the DFT results

Combining the results of the periodic DFT calculations (section 3a) with the information about the exposed surfaces obtained by low temperature CO adsorption (section 4a), we can now provide a complete assignment of the FTIR spectra of CO_2 adsorbed at room temperature on heavily dehydroxylated nanoanatase (**Figure 5**):

1) The band which dominates the IR spectrum (inset of **Figure 5**) is undoubtedly originated by the ν_{AS}(CO) of CO_2 linearly adsorbed on the (101) anatase surface (101-L1, see **Figure 2** and **Table 2-3**). This signal appears at 2357 cm^{-1} and shifts down to 2353 cm^{-1} before going out of scale at high coverage. Its broad character suggests the presence of a variety of slightly different binding configurations (e.g. 101-L2, 101-L3, 101-B, see **Figure 2**) in addition to the most stable one (101-L1). The ν_{AS}(CO) of the $^{13}CO_2$ isotope (natural abundance ~ 1%) can be detected at 2285 cm^{-1}.

2) Based on the literature,[19] the doublet centred at 1376 and 1268 cm^{-1} can be assigned to a Fermi resonance between the symmetric stretching, ν_{SS}(CO), and the first overtone of the deformation mode, $2\nu_B$(OCO), of CO_2 adsorbed on the (101) surface (101-L1, see **Figure 2).** This resonance is IR inactive in gaseous CO_2 and can be found at 1388 and 1285 cm^{-1} by Raman spectroscopy. These signals completely disappear together with the main band due to the ν_{AS}(CO) after outgassing at room temperature. Their reversible nature is in full agreement with the low calculated ΔE_{form} (-5.7 kcal mol^{-1}) for 101-L1 at θ = 1 (**Table 3**).

3) The most intense band in the 1800-1200 cm^{-1} region, initially centred at 1584 cm^{-1} and progressively shifting to 1587 cm^{-1} while increasing the coverage, can be assigned to the ν_{AS}(CO) of monodentate carbonates on the anatase (001) surface (001-MC, see **Figure 1** and **Table 1-4**). However, similar species can be formed also on the low coordinated sites located on edges, steps and corners, which have been highlighted by the preliminary CO adsorption (section 2a). Another ν_{AS}(CO) can be found at 1321 cm^{-1} at low coverage. This signal progressively shifts to 1316 cm^{-1} and its intensity grows in parallel to the ν_{AS}(CO) band as expected. These bands are still present even after prolonged outgassing at room temperature in agreement with the calculated ΔE_{form} of -30.1 kcal mol^{-1} for 001-MC at θ = 0.25 (**Table 1**).

4) The weak signals centred at 1673, 1434 and 1222 cm^{-1}, which appear only at higher CO_2 coverages, can be ascribed to surface mono and bidentate bicarbonates which are originated by the reaction of CO_2 with the few residual hydroxyl groups. Their assignment will be discussed in greater details in the following section which is devoted to the partially hydrated anatase surfaces.

5) FTIR spectroscopy of partially hydrated surfaces

a) Study of the exposed surface sites by CO adsorption

To investigate the effect of adsorbed water on the CO_2 interaction with anatase surfaces, we prepared a partially hydroxylated sample by re-adsorbing approximately half monolayer of water on a sample previously outgassed at 823 K. The presence of molecular water on the surface is testified by the appearance of the peak associated with the H_2O bending mode and by the strong and complex absorption in the OH region. In these conditions the less reactive faces are expected to be partially covered by molecular water coordinated to fivefold coordinated Ti^{4+} sites, while the most reactive faces, the edges, steps and corners are nearly fully hydroxylated.[13]

In order to obtain an accurate surface picture also of the partially hydrated material, we performed again a low temperature CO adsorption experiment before studying the interaction of CO_2. From **Figure 6** we can note the disappearance of the bands which were present at 2166 and 2208 cm^{-1} on the dehydroxylated surface (**Figure 4**). This observation suggests that the (001) surface and the low coordinated sites, located on steps, edges and corners, are now completely hydroxylated. This is further confirmed by the increased intensity of the broad band centred at 2153 cm^{-1} which is due to CO interacting with OH groups. Moreover, the intensity of the peak at 2179 cm^{-1}, ascribed to the (101) surface, is approximately halved with respect to the dehydroxylated surface. The reduced intensity of this band indicates that also part of the (101) surface is covered by molecular water.[13]

b) CO_2 adsorption and comparison with the DFT results

The knowledge of the surface Ti sites which are occupied by adsorbed water or hydroxyls in the partially hydrated sample, achieved using CO as probe molecule (section 5a), allows us to better understand the differences in the FTIR spectra of CO_2 adsorbed on heavily dehydroxylated (**Figure 5**) or partially hydrated (**Figure 7**) nanoanatase. The comparison of the two samples can further clarify the origin of the weak signals ascribed to surface bicarbonates and confirm the proposed spectral assignments. In particular, considering **Figure 7**, we can note that:

1) The peak originated by the $\nu_{AS}(CO)$ mode of CO_2 linearly adsorbed on the (101) anatase surface (101-L1, see **Figure 2** and **Table 2-3**) is still dominating the IR spectra, but its intensity is considerably reduced with respect to the heavily dehydroxylated sample (**Figure 5**). This is due to the fact that approximately half of the (101) surface is covered by molecular water, as highlighted by CO adsorption. Moreover, because of the presence of coadsorbed water, the main component of the band is now centred at 2344 cm^{-1}.

2) Owing to the molecular water present on the (101) surface, also the intensity of the doublet due to the $\nu_{SS}(CO)$-$2\nu_B(OCO)$ Fermi resonance of CO_2 adsorbed on the (101)

surface is dramatically reduced and only the component at 1378 cm^{-1} is now clearly observable.

3) The most intense band in the 1800-1200 cm^{-1} region is now initially centred at 1577 cm^{-1} and progressively shifts to 1586 cm^{-1} while increasing the coverage. Its intensity grows in parallel with the bands centred at 1432 cm^{-1} and at 1222 cm^{-1}. These signals were present also in the dehydroxylated sample, but they were weak: their increased intensity in the hydrated sample confirm their assignment to surface bicarbonates. More in detail, by comparison with the DFT calculations, we can ascribe them to the ν_{AS}(CO) and ν_{B}(COH) modes of bidentate bicarbonates similar to the 001-BB3 structure (see **Tables 4-5** and **Figure 3**). Other kinds of bidentate bicarbonates (like 001-BB1, 001-BB2, 001-BB4) can contribute to the shoulder of the main peak at about 1610 cm^{-1}. The intensity of all these bands can be considerably reduced after outgassing at room temperature in agreement with their calculated ΔE_{form} which ranges from -1.5 kcal mol^{-1} for 001-BB4 to -14.6 kcal mol^{-1} for 001-BB2 (**Table 4**).

4) The peak centred at 1317 cm^{-1}, originated by the ν_{AS}(CO) mode of monodentate carbonates (001-MC, see **Figure 1** and **Table 5**), is now very weak, as expected, since in the hydrated sample the (001) surface and the low coordinated sites, which readily form these kind of species in the dehydroxylated sample, are nearly fully covered by OH groups.

5) The bands centred at 1674 and 1245 cm^{-1} can be assigned to the ν_{AS}(CO) and ν_{B}(COH) modes of monodentate bicarbonates similar to the 001-MB1 structure (see **Table 5** and **Figure 1**). These signals are the first to disappear after short outgassing at room temperature confirming their assignment to labile species characterized by low ΔE_{form}.

Discussion and Conclusions

The comparison between experimental and DFT results performed in this work highlights an extraordinary different reactivity of the (101) and (001) anatase surfaces towards CO_2 adsorption. When the linear configuration is considered, CO_2 interacts through the oxygen end with the Ti Lewis acid sites. On both surfaces the interaction is rather weak and of comparable entity: ΔE_{form}=-9.5 and -5.3 kcal mol^{-1} for (101) and (001), respectively. The acidity of the (101) Lewis acid sites, as probed by CO_2, appears slightly stronger than the acidity of the (001) ones in agreement with the results obtained using CO.[17] The easier formation of carbonate moieties at the (001) surface must be therefore related to a stronger Lewis basicity of the two-fold oxygen centres with respect to those

exposed by the (101) face. The projected density of states (PDOSs) reported in **Figure 8** can shed light on the different behaviour of the surface sites of the two anatase surfaces. As in bulk anatase, the top of the valence band (VB) is characterized by O 2sp states, whereas the bottom of the conduction band (CB) by Ti 3d empty states. However, with respect to the (101) surface, the (001) exhibits the top of the VB considerably upshifted (by 0.7 eV) and with a major contribution from O(2f) states: these findings are the indicators of an enhanced basicity of the surface sites. In addition the Mulliken charges of O(2f) centres, -0.8 and -0.7 a.u. for (001) and (101) cases respectively, are consistent with the PDOS analysis. It is worth noticing that the higher Lewis basicity of (001) O(2f) sites is also accompanied by a higher Bronsted basicity as indicated by the capability of dissociate water even at very low coverage.[15]

The two bonding behaviour of CO_2 (linear and bent) are characterized by completely different bond mechanisms. PDOSs of **Figure 8** illustrate the electron structures of 101-L1 and 001-MC which can be considered explicative of the two bonding types. In the linear configuration, the CO_2 frontier orbitals, 1π (HOMO) and $2\pi^*$ (LUMO), are slightly downshifted with respect to the free molecule but retain their structure indeed confirming the formation of a weak interaction mainly of electrostatic nature. In a free CO_2 frozen in a bent configuration by keeping fixed the angle at the same value that the molecule adopts in the adsorbed state, the 1π and the $2\pi^*$ are split into the $1a_2$, and $4a_2$ and into $6a_1$ and $2b_1$, respectively. The most relevant feature of the interaction is the downshift of the $6a_1$ orbital below the Fermi level, and the strong coupling with the 2sp states of surface oxygens, thus indicating the formation of a strong covalent bond. At the interface electron charge is transferred from anatase to the CO_2 states, as documented by the downshift of the TiO_2 VB by 0.85 eV, **Figure 8**. The charged nature of the adsorbates is also proven by Mulliken charges: the surface $–CO_2$ moieties bear a charge of -0.7 au; this finding explains the remarkable increase of ΔE_{form} by decreasing the surface coverage, highlighted in the previous section, as due to electrostatic repulsion between charged adsorbates.

Simulated spectra have been constructed by employing computed IR data of the structures considered the most likely on the basis of the results discussed in the previous sections and namely: 101-L1 and 001-MC to describe the formation of linear adsorbates and carbonate species at the (101) and (001) dehydrated surfaces; 001-BB2, 001-BB3 and 001-MB1 as the most representative of bicarbonates at the (001) hydrated surface (see **Figure 9**). The agreement between experimental and computed spectra is satisfactory and makes us confident that each surface species provides a fingerprint that can be successfully used for its recognition.

To summarize, in this work we have highlighted the role of the different TiO_2 surface sites in the CO_2 adsorption and in the subsequent reactions. We have highlighted that the formation of

carbonate and bicarbonate species occurs preferentially on the anatase (001) surface and the higher reactivity of this surface is related to a stronger (Lewis and Brønsted) basicity of the surface oxygen sites. On the contrary, at the most stable (101) surface CO_2 is weakly adsorbed and retains its molecular properties. Hydroxylated low coordinated sites can play an important role to stabilize monodentated bicarbonates.

We showed that our (1x1) model for the (001) surface can satisfactorily reproduce the spectroscopic features of CO_2 adsorbed on nanoanatase, confirming the results previously obtained for CO.[13,17,35] However in the future we plan to extend our study also to the (1x4) reconstruction of the anatase (001) surface, which has been reported to be the most common.[36,37]

The results presented in this paper can be extremely useful to rationally guide the synthesis of TiO_2 nanoparticles which preferentially expose the most suitable surface for the desired application. Indeed, in the last years crystal facet engineering of semiconductors has become an important strategy for fine-tuning the physicochemical properties and thus optimizing the reactivity and selectivity of photocatalysts.[38] Our findings suggest that a controlled variation of the exposed anatase surfaces can modify the reaction paths and favour the formation of the desired chemicals.

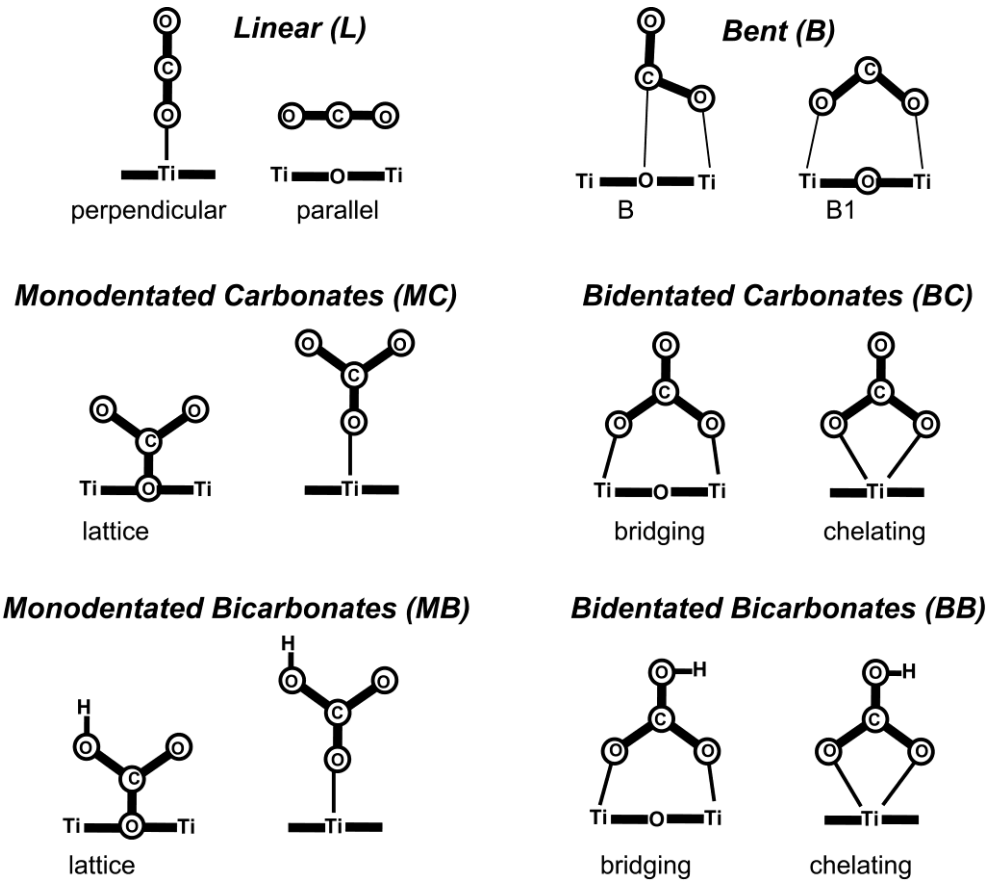

Scheme 1. Possible surface structures of CO_2 on TiO_2 surfaces.

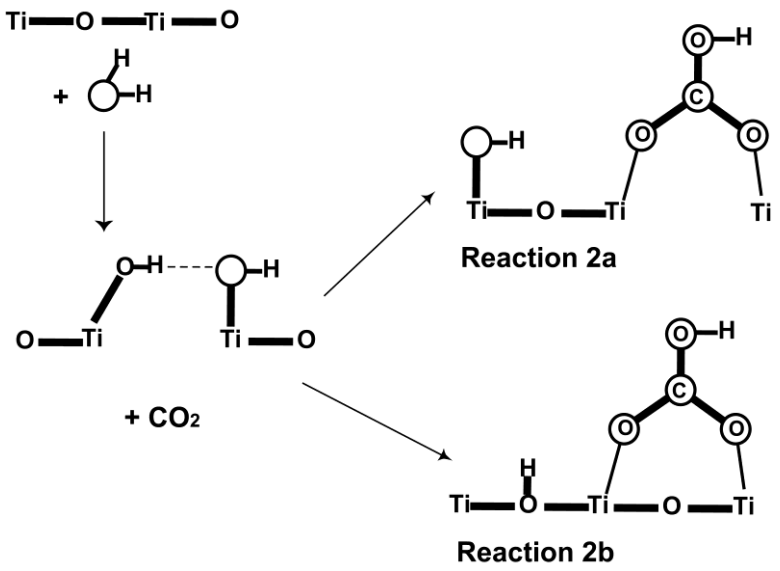

Scheme 2. Possible reactions of CO_2 with TiO_2 surface hydroxyls to form bicarbonates.

Table 1. Computed properties, using the PBE0 functional, of the CO_2 adsorption on the (001) anatase surface at different coverages θ. Bond distances, d, in Å; bond angles, α, in degrees; formation energy, ΔE_{form}, in kcal mol^{-1}. See also **Figure 1.**

System	001-L1	001-L2	001-MC		001-BC
θ	*0.25*	*1*	*0.25*	*0.5*	*0.25*
d(Ti-O)	3.402	2.924	2.054	2.049	1.803 1.815
$d(O_S$-C)	2.858	3.417	1.307	1.313	1.338 1.330
d(C-O) (*)	1.157	1.155 1.158	1.265 1.262	1.261 1.261	1.187
α(O-C-O) (*)	177.8	179.0	130.7	131.4	135.0
α(Ti-O-C)	107.4	130.3	92.6	92.6	155.4
ΔE_{form} (**)	-5.31	-3.41	-30.1	-27.3	-20.9

(*) For free CO_2: d(C-O)=1.157 Å; α(O-C-O)=180°

(**)$\Delta E_{form} = E(TiO_2/CO_2) - E(TiO_2) - E(CO_2)$

Table 2. Main IR vibrational frequencies (ν in cm^{-1}) of relevant linear CO_2 surface adducts computed using the PBE0 functional. In brackets the intensity of each mode in km mol^{-1} is reported. ν_{AS} and ν_{SS} are the symmetric and asymmetric stretchings; ν_B are angle bendings. All frequencies have been scaled of a factor 0.9525 in order to match the experimental and computed data in gas phase. See also **Figures 1-2**.

	CO_2	101-L1		101-L2	001-L1	001-L2
θ	*gas phase*	*0.25*	*1*	*0.25*	*0.25*	*1*
ν_{AS}(CO)	2349 (77)	2359 (1573)	2369 (1443)	2360 (1364)	2336 (1658)	2354 (875)
ν_{SS}(CO)	1335 (0)	1340 (14)	1346 (8)	1336 (8)	1332 (1)	1337 (1)
ν_B(OCO)	652 (694)	642 (108)	650 (103)	652 (98)	648 (98)	654 (53)
		641 (107)	635 (126)	648 (88)	640 (127)	639 (73)

Table 3. Computed properties, using the PBE0 functional, of the CO_2 adsorption on the (101) anatase surface at different coverages θ. Bond distances, d, in Å; bond angles, α, in degrees; formation energy, ΔE_{form}, in kcal mol^{-1}. See also **Figure 2**.

System	101-L1		101-L2	101-L3	101-B		101-MC
θ	*0.25*	*1*	*0.25*	*0.25*	*0.25*	*1*	*0.25*
d(Ti-O)	2.620	2.670	2.543	2.40	1.904	1.871	2.185
$d(O_S$-C)	3.098	3.109	2.992	3.341	1.375	1.396	1.417
d(C-O)(*)	1.162 1.150	1.161 1.152	1.163 1.150	1.162 1.150	1.322 1.182	1.329 1.172	1.234 1.234
α(O-C-O)(*)	177.6	177.4	178.7	179.0	130.2	131.4	136.9
α(Ti-O-C)	148.9	148.7	125.9	134.1	101.3	101.3	-
ΔE_{form} (**)	-9.5	-5.7	-7.8	-8.5	2.7	7.6	7.3

(*) For free CO_2: d(C-O)=1.157 Å; α(O-C-O)=180°

(**)$\Delta E_{form} = E(TiO_2/CO_2) - E(TiO_2) - E(CO_2)$

Table 4. Main IR vibrational frequencies (ν in cm^{-1}) of relevant surface carbonates and bicarbonates, computed using the PBE0 functional. In brackets the intensity of each mode in km mol^{-1} is reported. ν_{AS} and ν_{SS} are the symmetric and asymmetric stretchings; ν_B are angle bendings. All frequencies have been scaled of a factor 0.9525 in order to match the experimental and computed data in gas phase. See also **Figures 1-3**.

	001-MC	**001-BC**	**001-BB1**	**001-BB2**	**001-BB3**	**001-BB4**	**001-MB1**
θ	*0.25*	*0.25*	*0.25*	*0.25*	*0.25*	*0.25*	*0.25*
ν_{AS}(CO)	1584 (3232) 1378 (214)	1802 (840) 1125 (1964) 1105 (4383)	1625 (4752) 1497 (951)	1625 (2903) 1448 (1312)	1574 (2054) 1426 (1162)	1613 (819) 1505 (993)	1656 (2181) 1432 (1063)
ν_{SS}(CO)	1058 (9)	-	1117 (2)	1068 (5)	1063 (2)	1048 (36)	1052 (125)
ν_B(OCO)	663 (23)	610 (6)	645 (16)	664 (13)	670 (18)	713 (66)	664 (31)
ν_B(COH)	-	-	1230 (293)	1218 (401)	1212 (276)	1193 (318)	1207 (516)

Table 5. Computed properties, using the PBE0 functional, of bicarbonates on the (001) anatase surface (θ=0.25). Bond distances, d, in Å; bond angles, α, in degrees; formation energy, ΔE_{form}, in kcal mol^{-1}. See also **Figure 3.**

system	**001-BB1**	**001-BB2**	**001-BB3**	**001-BB4**	**001-MB1**	**001-MB2**	**001-MB3**
d(O-H)	0.966	0.965	0.966	0.965	0.965	0.964	0.974
$d(O_S\text{-}OH)$	-	-	-	-	1.573	-	1.854
d(Ti-O)	1.958	2.038	2.065	2.161	1.951	1.924	1.854
	1.982	2.054	2.067				
$d(O_S\text{-}C)$	-	2.994	2.788	-	2.925	3.026	3.198
d(C-O)	1.319	1.254	1.254	1.253	1.229	1.206	1.188
	1.247	1.261	1.265	1.259	1.279	1.310	1.328
	1.253	1.337	1.332	1.325	1.337	1.349	1.358
α(O-C-O)	114.6	115.4	116.2	119.3	113.2	109.8	113.0
	115.9	116.2	118.3	119.6	120.8	122.4	122.2
	129.5	128.0	125.5	121.1	126.0	127.8	124.9
α(C-O-H)	107.0	107.2	107.7	107.4	106.4	106.1	107.9
α(Ti-O-C)	135.8	137.6	143.1	89.9	146.7	135.7	147.4
$\Delta E_{form}{}^{(*)}$	-10.3	-14.6	-4.3	-1.5	0.1	3.5	8.6

$^{(*)}\Delta E_{form} = E((TiO_2)_{hyd}/CO_2) - E((TiO_2)_{hyd}) - E(CO_2)$

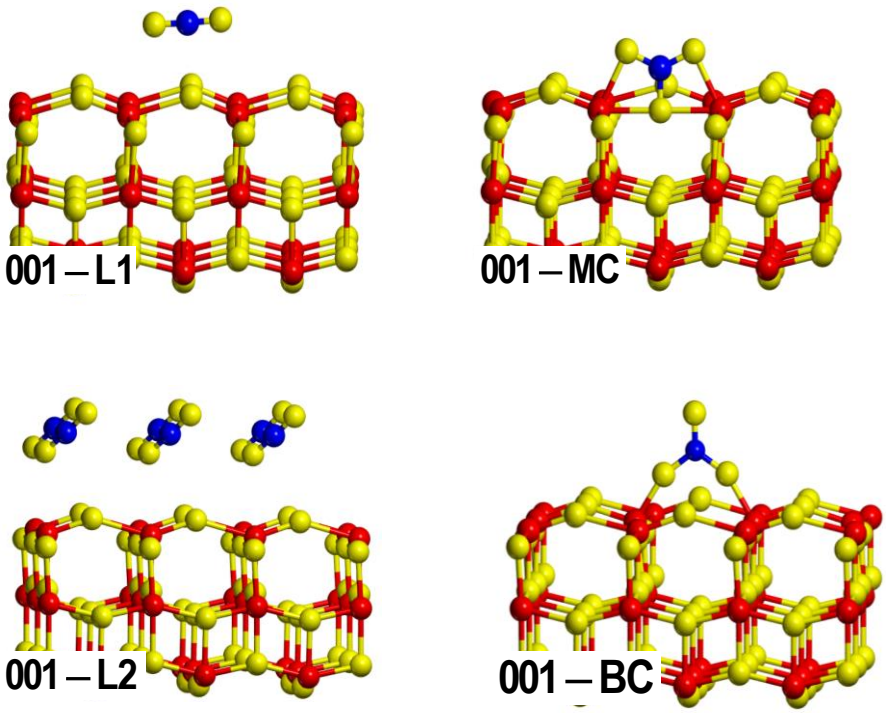

Figure 1. Investigated CO_2 adsorption geometries on the anatase (001) surface. Oxygen, titanium, and carbon atoms are represented in yellow, red, and blue, respectively.

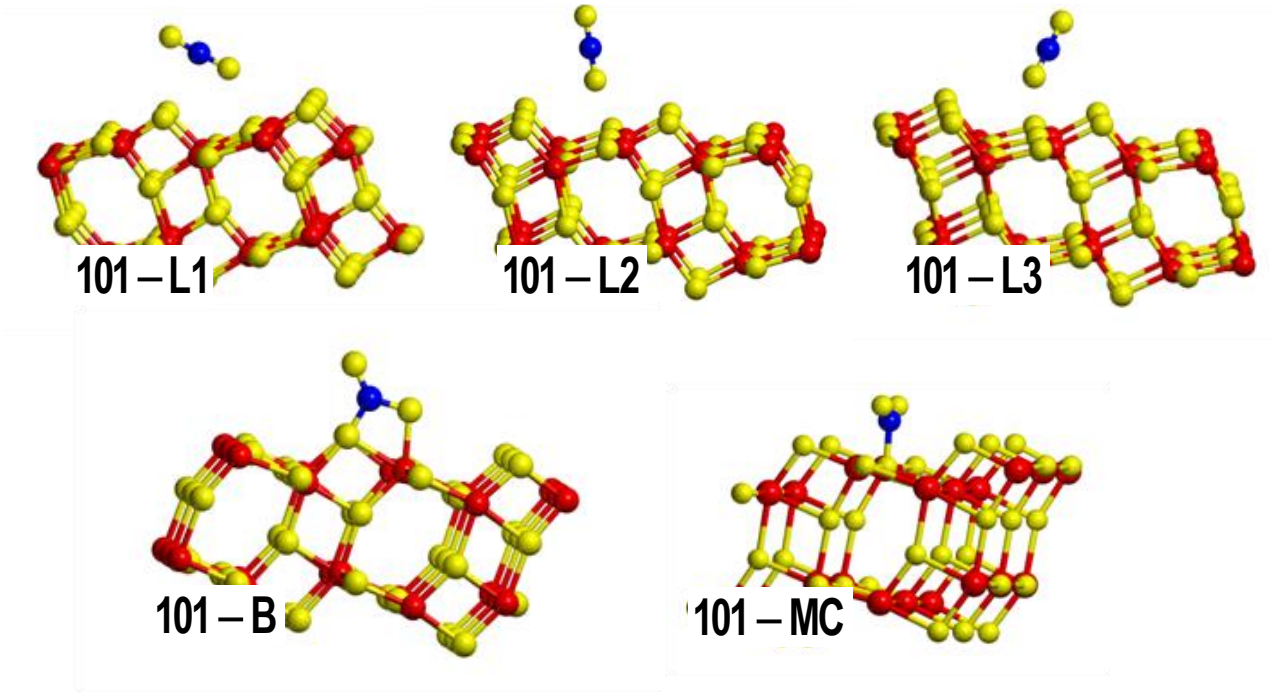

Figure 2. Investigated CO_2 adsorption geometries on the anatase (101) surface. Oxygen, titanium, and carbon atoms are represented in yellow, red, and blue, respectively.

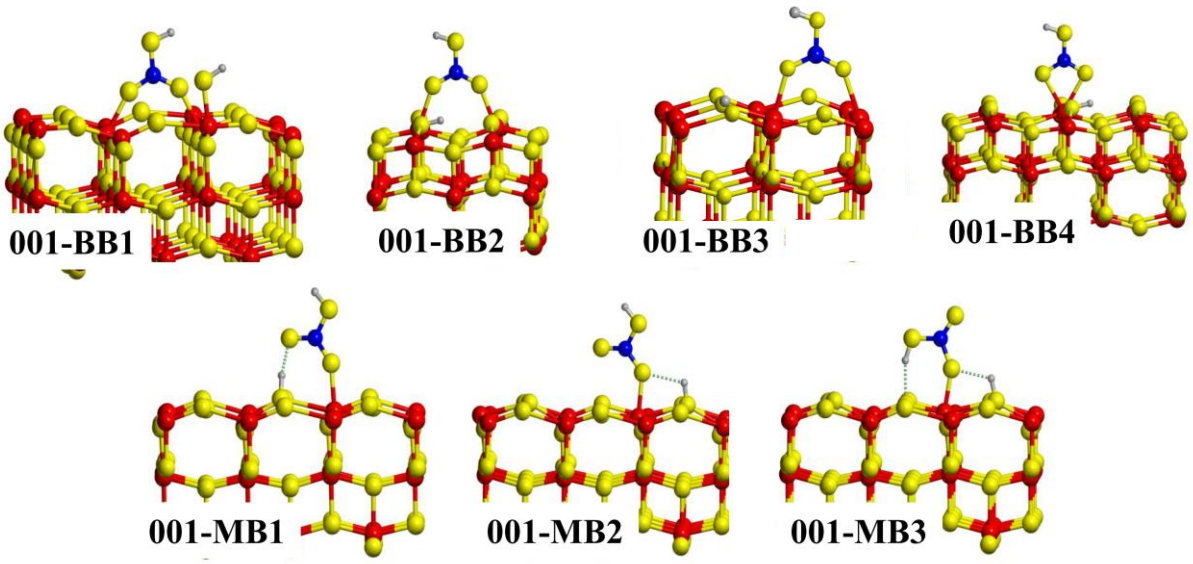

Figure 3. Investigated bicarbonates on the anatase (001) surface. Oxygen, titanium, carbon and hydrogen atoms are represented in yellow, red, blue and grey, respectively.

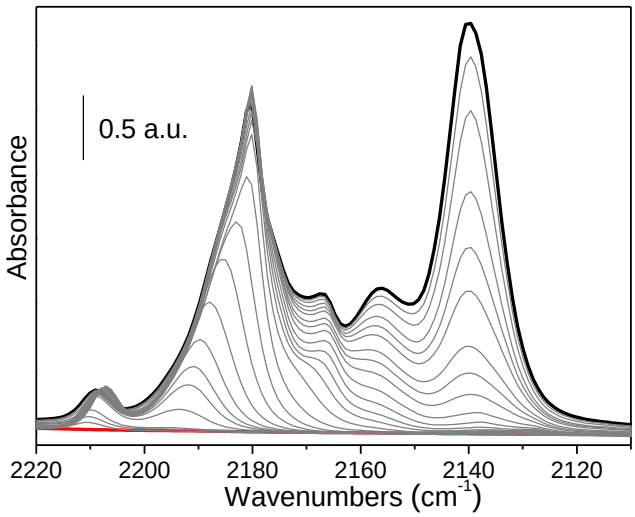

Figure 4. FTIR spectra, recorded at 60 K, of CO adsorbed at progressively decreasing coverages on nanoanatase previously outgassed at 823 K. The black curve refers to the maximum coverage (40 mbar), the red curve to complete CO outgassing.

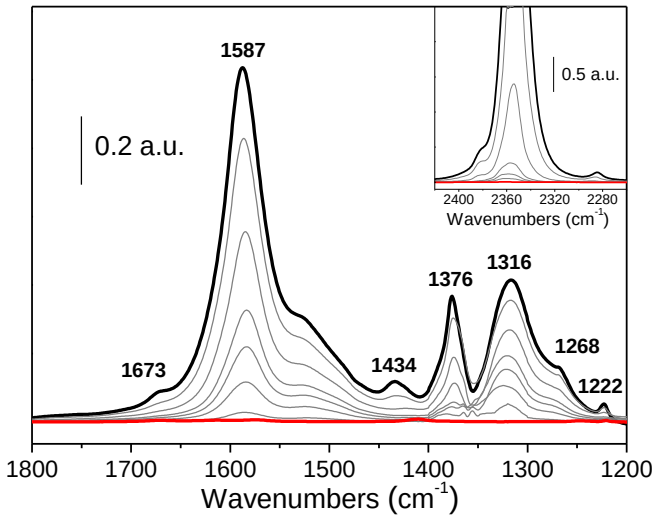

Figure 5. FTIR spectra, recorded at room temperature, of CO_2 adsorbed at progressively increasing coverages on nanoanatase previously outgassed at 823 K. The spectrum of the activated material has been subtracted from all spectra. The black curve refers to the maximum coverage (10 mbar of CO_2), the red curve to the material before sending CO_2. In the inset the CO_2 asymmetric stretching mode spectral region is reported.

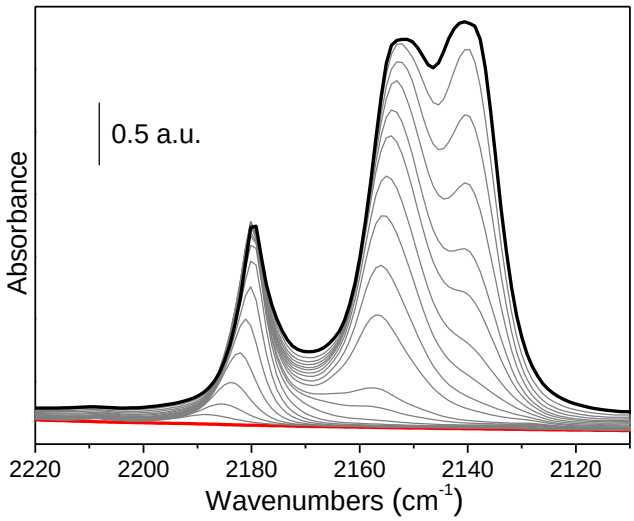

Figure 6. FTIR spectra, recorded at 60 K, of CO adsorbed at progressively decreasing coverages on nanoanatase previously outgassed at 823 K and then partially rehydrated. The black curve refers to the maximum coverage (40 mbar), the red curve to complete CO outgassing.

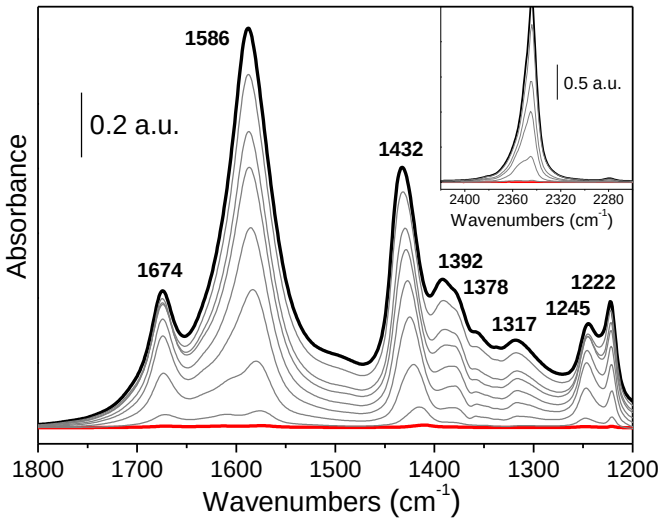

Figure 7. FTIR spectra, recorded at room temperature, of CO_2 adsorbed at progressively increasing coverages on nanoanatase previously outgassed at 823 K and then partially rehydrated. The spectrum of the rehydrated material has been subtracted from all spectra. The black curve refers to the maximum coverage (10 mbar of CO_2), the red curve to the material before sending CO_2. In the inset the CO_2 asymmetric stretching mode spectral region is reported.

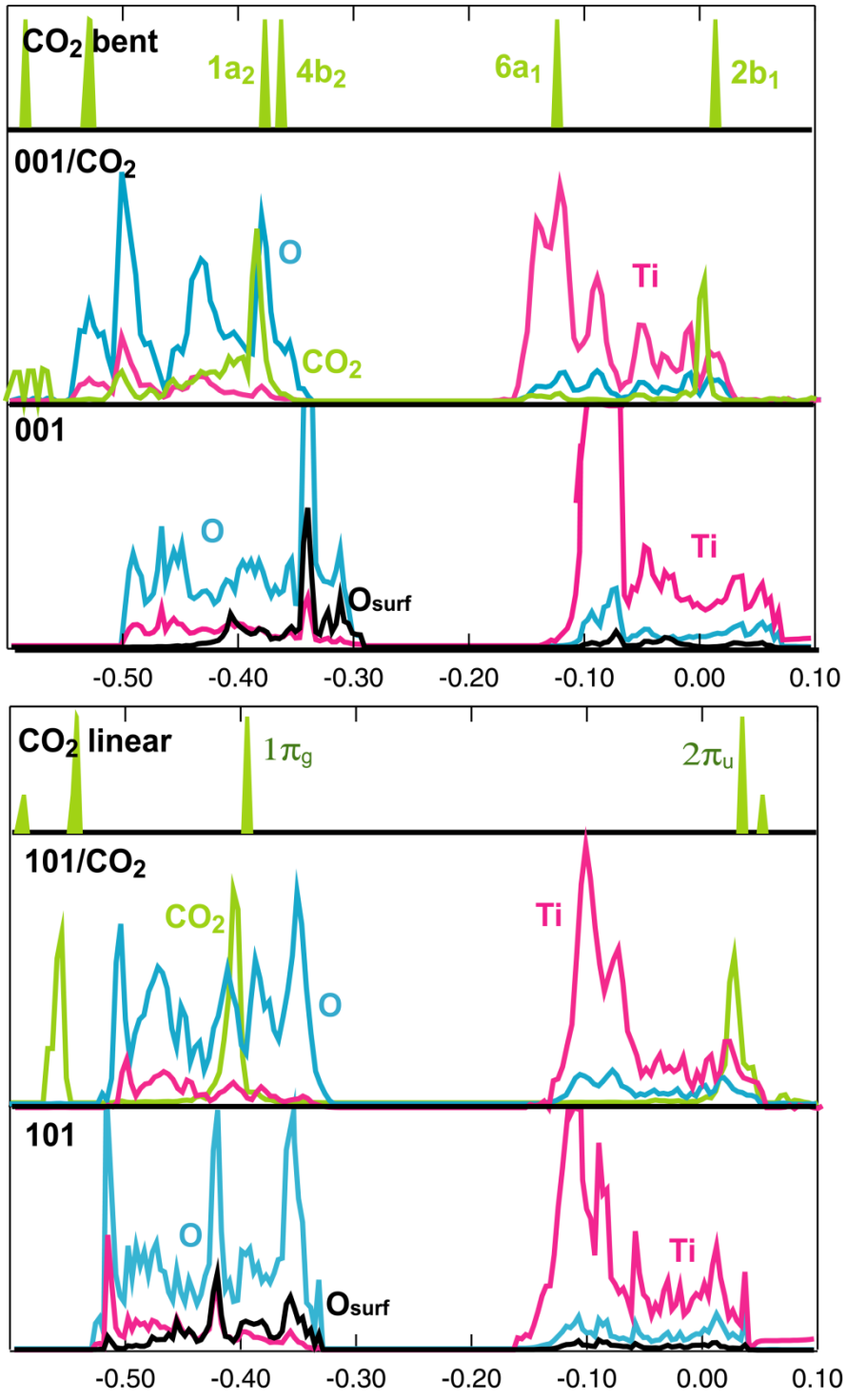

Figure 8. PDOS of 101-L1 (bottom panels) and 001-MC (top panels) systems compared to the reference bare surfaces and free CO_2. The bent free CO_2 has been optimized keeping fixed the angle at the same value adopted in the surface configuration. The zero of energy corresponds to the vacuum level. Energy in Hartree.

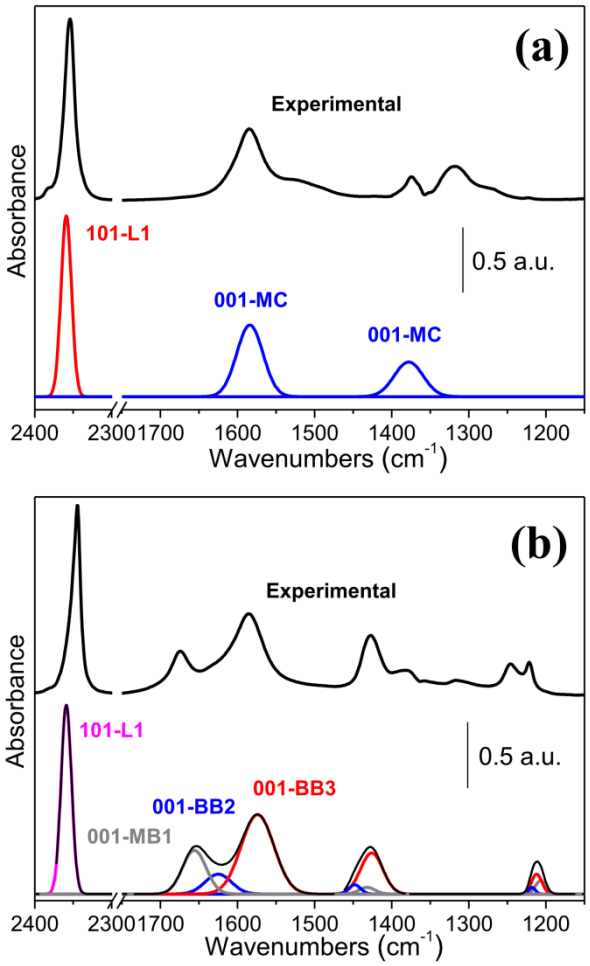

Figure 9. Comparison between experimental and simulated IR spectra constructed employing computed IR data for the dehydrated (part a) and partially hydrated (part b) anatase surfaces. The structures considered are the most likely on the basis of the analysis performed in the previous sections.

References

(1) Balzani, V.; Credi, A.; Venturi, M. Photochemical Conversion of Solar Energy *ChemSusChem* **2008**, *1*, 26-58.

(2) Harvey, O. R.; Qafoku, N. P.; Cantrell, K. J.; Lee, G.; Amonette, J. E.; Brown, C. F. Geochemical Implications of Gas Leakage Associated with Geologic CO_2 Storage-a Qualitative Review *Environ. Sci. Technol.* **2013**, *47*, 23-36.

(3) D'Alessandro, D. M.; Smit, B.; Long, J. R. Carbon Dioxide Capture: Prospects for New Materials *Angew. Chem.-Int. Edit.* **2010**, *49*, 6058-6082.

(4) Habisreutinger, S. N.; Schmidt-Mende, L.; Stolarczyk, J. K. Photocatalytic Reduction of CO_2 on TiO_2 and Other Semiconductors *Angew. Chem.-Int. Edit.* **2013**, *52*, 7372-7408.

(5) Inoue, T.; Fujishima, A.; Konishi, S.; Honda, K. Photoelectrocatalytic Reduction of Carbon Dioxide in Aqueous Suspensions of Semiconductor Powders *Nature* **1979**, *277*, 637-638.

(6) Anpo, M.; Yamashita, H.; Ichihashi, Y.; Ehara, S. Photocatalytic Reduction of CO_2 with H_2O on Various Titanium-Oxide Catalysts *J. Electroanal. Chem.* **1995**, *396*, 21-26.

(7) Wu, J. C. S. Photocatalytic Reduction of Greenhouse Gas CO_2 to Fuel *Catal. Surv. Asia* **2009**, *13*, 30-40.

(8) Roy, S. C.; Varghese, O. K.; Paulose, M.; Grimes, C. A. Toward Solar Fuels: Photocatalytic Conversion of Carbon Dioxide to Hydrocarbons *ACS Nano* **2010**, *4*, 1259-1278.

(9) Li, G. H.; Ciston, S.; Saponjic, Z. V.; Chen, L.; Dimitrijevic, N. M.; Rajh, T.; Gray, K. A. Synthesizing Mixed-Phase TiO_2 Nanocomposites Using a Hydrothermal Method for Photo-Oxidation and Photoreduction Applications *J. Catal.* **2008**, *253*, 105-110.

(10) Varghese, O. K.; Paulose, M.; LaTempa, T. J.; Grimes, C. A. High-Rate Solar Photocatalytic Conversion of CO_2 and Water Vapor to Hydrocarbon Fuels *Nano Lett.* 2009, *9*, 731-737.

(11) Sorescu, D. C.; Al-Saidi, W. A.; Jordan, K. D. CO_2 Adsorption on TiO_2(101) Anatase: A Dispersion-Corrected Density Functional Theory Study *J. Chem. Phys.* 2011, *135*, 17.

(12) Sorescu, D. C.; Lee, J.; Al-Saidi, W. A.; Jordan, K. D. CO_2 Adsorption on TiO_2(110) Rutile: Insight from Dispersion-Corrected Density Functional Theory Calculations and Scanning Tunneling Microscopy Experiments *J. Chem. Phys.* **2011**, *134*, 12.

(13) Mino, L.; Spoto, G.; Bordiga, S.; Zecchina, A. Particles Morphology and Surface Properties as Investigated by HRTEM, FTIR, and Periodic DFT Calculations: From Pyrogenic TiO_2 (P25) to Nanoanatase *J. Phys. Chem. C* **2012**, *116*, 17008-17018.

(14) Deiana, C.; Minella, M.; Tabacchi, G.; Maurino, V.; Fois, E.; Martra, G. Shape-Controlled TiO_2 Nanoparticles and TiO_2 P25 Interacting with CO and H_2O_2 Molecular Probes: A Synergic Approach for Surface Structure Recognition and Physico-Chemical Understanding *Phys. Chem. Chem. Phys* **2013**, *15*, 307-15.

(15) Vittadini, A.; Selloni, A.; Rotzinger, F. P.; Gratzel, M. Structure and Energetics of Water Adsorbed at TiO_2 Anatase (101) and (001) Surfaces *Phys. Rev. Lett.* **1998**, *81*, 2954-2957.

(16) Onal, I.; Soyer, S.; Senkan, S. Adsorption of Water and Ammonia on Tio2-Anatase Cluster Models *Surf. Sci.* **2006**, *600*, 2457-2469.

(17) Mino, L.; Ferrari, A. M.; Lacivita, V.; Spoto, G.; Bordiga, S.; Zecchina, A. CO Adsorption on Anatase Nanocrystals: A Combined Experimental and Periodic DFT Study *J. Phys. Chem. C* **2011**, *115*, 7694-7700.

(18) Busca, G.; Lorenzelli, V. Infrared Spectroscopic Identification of Species Arising from Reactive Adsorption of Carbon Oxides on Metal Oxide Surfaces *Mater. Chem.* **1982**, *7*, 89-126.

(19) Ramis, G.; Busca, G.; Lorenzelli, V. Low-Temperature CO_2 Adsorption on Metal-Oxides - Spectroscopic Characterization of Some Weakly Adsorbed Species *Mater. Chem. Phys.* **1991**, *29*, 425-435.

(20) Martra, G. Lewis Acid and Base Sites at the Surface of Microcrystalline TiO_2 Anatase: Relationships between Surface Morphology and Chemical Behaviour *Appl. Catal. A-Gen.* **2000**, *200*, 275-285.

(21) Liao, L. F.; Lien, C. F.; Shieh, D. L.; Chen, M. T.; Lin, J. L. FTIR Study of Adsorption and Photoassisted Oxygen Isotopic Exchange of Carbon Monoxide, Carbon Dioxide, Carbonate, and Formate on TiO_2 *J. Phys. Chem. B* **2002**, *106*, 11240-11245.

(22) Dovesi, R.; Saunders, V. R.; Roetti, C.; Orlando, R.; Zicovich-Wilson, C. M.; Pascale, F.; Civalleri, B.; Doll, K.; Harrison, N. M.; Bush, I. J.*et al.* Crystal09 User's Manual *CRYSTAL09 User's Manual* **2009**, *University of Torino*.

(23) Adamo, C.; Barone, V. Toward Reliable Density Functional Methods without Adjustable Parameters: The PBE0 Model *J. Chem. Phys.* **1999**, *110*, 6158-6170.

(24) Labat, F.; Baranek, P.; Adamo, C. Structural and Electronic Properties of Selected Rutile and Anatase TiO_2 Surfaces: An Ab Initio Investigation *J. Chem. Theory Comput.* **2008**, *4*, 341-352.

(25) Hay, P. J.; Wadt, W. R. Ab Initio Effective Core Potentials for Molecular Calculations. Potentials for the Transition Metal Atoms Sc to Hg *J. Chem. Phys.* **1985**, *82*, 270-283.

(26) Spurr, R. A.; Myers, H. Quantitative Analysis of Anatase-Rutile Mixtures with an X-Ray Diffractometer *Anal. Chem.* **1957**, *29*, 760-762.

(27) Indrakanti, V. P.; Kubicki, J. D.; Schobert, H. H. Quantum Chemical Modeling of Ground States of CO_2 Chemisorbed on Anatase (001), (101), and (010) TiO_2 Surfaces *Energy Fuels* **2008**, *22*, 2611-2618.

(28) Pipornpong, W.; Wanbayor, R.; Ruangpornvisuti, V. Adsorption CO_2 on the Perfect and Oxygen Vacancy Defect Surfaces of Anatase TiO_2 and Its Photocatalytic Mechanism of Conversion to CO *Appl. Surf. Sci.* **2011**, *257*, 10322-10328.

(29) Cornu, D.; Guesmi, H.; Krafft, J. M.; Lauron-Pernot, H. Lewis Acido-Basic Interactions between CO_2 and Mgo Surface: DFT and DRIFT Approaches *J. Phys. Chem. C* **2012**, *116*, 6645-6654.

(30) He, H. Y.; Zapol, P.; Curtiss, L. A. A Theoretical Study of CO_2 Anions on Anatase (101) Surface *J. Phys. Chem. C* **2010**, *114*, 21474-21481.

(31) He, H. Y.; Zapol, P.; Curtiss, L. A. Computational Screening of Dopants for Photocatalytic Two-Electron Reduction of CO_2 on Anatase (101) Surfaces *Energy Environ. Sci.* **2012**, *5*, 6196-6205.

(32) Prencipe, M.; Pascale, F.; Zicovich-Wilson, C. M.; Saunders, V. R.; Orlando, R.; Dovesi, R. The Vibrational Spectrum of Calcite ($CaCO_3$): An Ab Initio Quantum-Mechanical Calculation *Phys. Chem. Miner.* **2004**, *31*, 559-564.

(33) Sun, C.; Liu, L.-M.; Selloni, A.; Lu, G. Q.; Smith, S. C. Titania-Water Interactions: A Review of Theoretical Studies *J. Mater. Chem.* **2010**, *20*, 10319-10334.

(34) Ye, J. Y.; Liu, C. J.; Ge, Q. DFT Study of CO_2 Adsorption and Hydrogenation on the In_2O_3 Surface *J. Phys. Chem. C* **2012**, *116*, 7817-7825.

(35) Mino, L.; Spoto, G.; Bordiga, S.; Zecchina, A. Rutile Surface Properties Beyond the Single Crystal Approach: New Insights from the Experimental Investigation of Different Polycrystalline Samples and Periodic DFT Calculations *J. Phys. Chem. C* **2013**, *117*, 11186-11196.

(36) Diebold, U. The Surface Science of Titanium Dioxide *Surf. Sci. Rep.* **2003**, *48*, 53-229.

(37) Xia, Y. B.; Zhu, K.; Kaspar, T. C.; Du, Y. G.; Birmingham, B.; Park, K. T.; Zhang, Z. R. Atomic Structure of the Anatase TiO_2(001) Surface *J. Phys. Chem. Lett.* **2013**, *4*, 2958-2963.

(38) Liu, G.; Yu, J. C.; Lu, G. Q.; Cheng, H. M. Crystal Facet Engineering of Semiconductor Photocatalysts: Motivations, Advances and Unique Properties *Chem. Commun.* **2011**, *47*, 6763-6783.

graphical abstract